Medical Engineering and Physics 111 (2023) 103927

Contents lists available at ScienceDirect

Medical Engineering and Physics

journal homepage: www.elsevier.com/locate/medengphy

The contribution of multibody optimization when using inertial measurement units to compute lower-body kinematics

Léonie Pacher [a], Nicolas Vignais [b], Christian Chatellier [c], Rodolphe Vauzelle [c], Laetitia Fradet [a,*]

[a] Equipe Robotique, Biomécanique, Sport, Santé, Institut PPRIME, UPR3346 CNRS Université de Poitiers ENSMA, Poitiers, 11, Boulevard Marie et Pierre Curie, Site du Futuroscope, F-86073 POITIERS CEDEX 9, France
[b] Complexity, Innovation, Sports & Motor Activities (CIAMS) laboratory, Université Paris-Saclay, 91405 Orsay cedex, France
[c] Equipe SYstèmes et réseaux de COMmunications Optique et Radio, Institut XLIM UMR CNRS 7252, Poitiers, 11, Boulevard Marie et Pierre Curie, Site du Futuroscope, F-86073 POITIERS CEDEX 9, France

ARTICLE INFO

Keywords:
Lower-body kinematics
Inertial measurement units
Multibody optimisation
Gait

ABSTRACT

Kinematics obtained using Inertial Measurement Units (IMUs) still present significant differences when compared to those obtained using optoelectronic systems. Multibody Optimization (MBO) might diminish these differences by reducing soft-tissue artefacts - probably emphasized when using IMUs - as established for optoelectronic-based kinematics.

To test this hypothesis, 15 subjects were equipped with 7 IMUs and 38 reflective markers tracked by 18 optoelectronic cameras. The subjects walked, ran, cycled on an ergocycle, and performed a task which induced joint movements in the transverse and frontal planes.

In addition to lower-body kinematics computed using the optoelectronical system data, three IMU-based kinematics were computed: from IMU orientations without MBO; from MBO performed using the OpenSense add-on of the OpenSim software (OpenSim 4.2, Stanford, USA); as outputs from the commercialised MVN MBO (Xsens, Netherlands). Root Mean Square Errors (RMSE), coefficients of correlations, and differences in range of motion were calculated between the three IMU-based methods and the reference kinematics.

MVN MBO seems to present a slight advantage over Direct kinematics or OpenSense MBO, since it presents 34 times out of 48 (12 degrees of freedom * 4 sports activities) a mean RMSE inferior to the Direct and OpenSense kinematics. However, it was not always significant and the differences rarely exceeded 2°. This study does not therefore conclude on a significant contribution of MBO in improving lower-body kinematics obtained using IMUs. This lack of results can partly be explained by the weakness of both the kinematic constraints applied to the kinematic chain and segment stiffening. Personalization of the kinematic chain, the use of more than one IMU by segment in order to provide information redundancy, or the use of other approaches based on the Kalman Filter might increase this MBO impact.

Table of acronyms

IMU	Inertial Measurement Unit
MBO	Multibody optimization
RMSE	Root Mean Square Error
CC	Pearson Correlation Coefficient
RoMdiff	absolute differences in range of motion
D	Direct
OS	OpenSense
X	Xsense
L	Longitudinal
ML	Mediolateral
V	Vertical
Seg	Segment
dist	Distal
prox	Proximal
dir mvt	Movement direction

1. Introduction

In order to perform human movement kinematics analyses outside laboratories, Inertial Measurement Units (IMUs) constitute a widely

* Corresponding author.
E-mail address: laetitia.fradet@univ-poitiers.fr (L. Fradet).

https://doi.org/10.1016/j.medengphy.2022.103927
Received 31 May 2022; Received in revised form 15 November 2022; Accepted 16 November 2022
Available online 30 December 2022

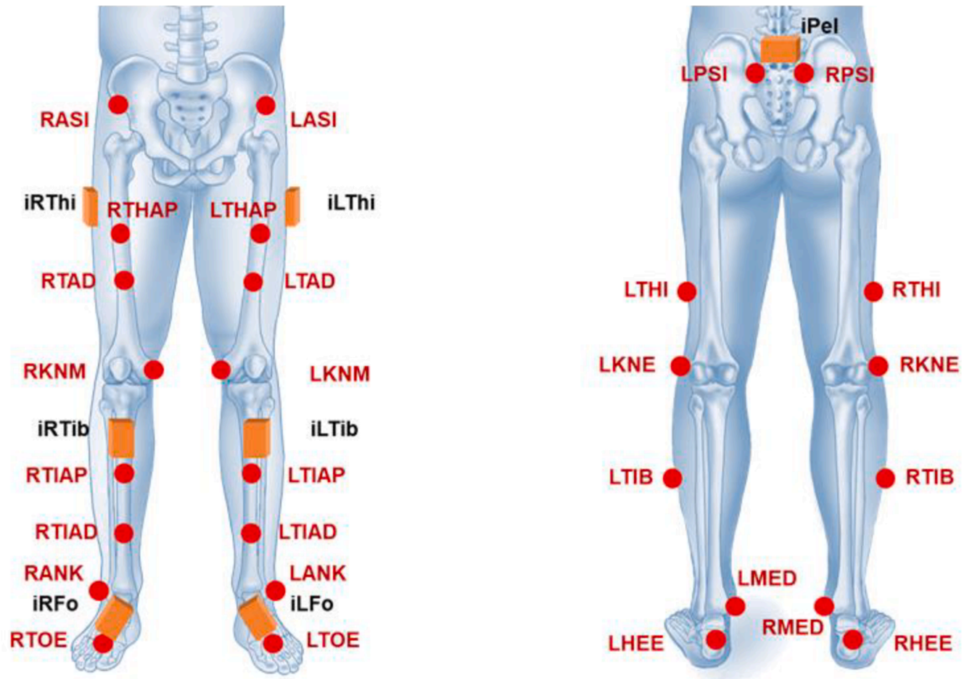

Fig. 1. Reflective markers used in the present study (following the Conventional Gait Model 2 [18]) and IMU placement.

adopted solution (see [1,2] for recent reviews). However, the related methodology seems to remain perfectible since errors of around 5° to 10°, in terms of root mean square errors, are seen when comparing joint kinematics obtained with IMUs with kinematics obtained with optoelectronic systems [3,4]. Of course, the reference used is questionable since optoelectronic methodologies are also imperfect because they are subject to various errors due to the use of external markers. Amongst these errors, the soft-tissue artefact to which these external markers are subject [5], marker misplacement [6], and the underlying model proposed to define the segment functional centres and axes from external information [7] may be cited.

When looking carefully at the lower-body kinematics obtained with IMUs, worse results in terms of pattern respect are found in the frontal and transverse planes compared to the sagittal plane [3,4]. A similar phenomenon is also seen when using optoelectronic systems, phenomenon that is mostly attributed to the soft-tissue artefact [8]. Given the fact that IMUs are bulkier and heavier devices than reflective markers – an IMU typically weighs more than 20 g compared with only a few grams for a reflective marker – they can therefore be particularly sensitive to soft-tissue artefacts.

A solution frequently used to limit these artefacts in motion analysis is multibody optimisation (MBO) [9,10]. The principle is to minimize the difference between measured and model-derived kinematics in order to estimate body-segment positions and orientations - the model being a kinematic chain representing the osteo-articular system (see [9] for a review). In popular software such as OpenSim [11], the model-derived kinematics is obtained by constrained optimisation, but Kalman filtering is also a possibility. Although different proposals have been made in the literature to apply MBO to IMU-measured data [9,12–14], it is not possible to evaluate the real benefit of this optimization on the lower-body joint kinematics. Indeed, the authors propose to compare their method to reference data obtained via optoelectronic systems and not to kinematics obtained “directly” with IMUs: in other words, without being submitted to MBO.

In the present study, we propose to compare two MBO methods based on IMU measures: the MVN model from the Xsens company (Enschede, the Netherlands) and the OpenSense add-on of the OpenSim musculoskeletal modelling software (Stanford, USA). The MVN model is part of a commercialized IMU-based motion-capture system that has its own protocols [14]. The lower-body kinematics obtained with this model were compared to optoelectronic-based reference kinematics during various locomotion modes, such as walking on level ground or stairs [15,16], jumps, or squats [15]. However, this proprietary model is not clearly defined in terms of constraints, optimization formulation, or sensor–to-segment calibration method. It was then decided to evaluate a second, open source, free, and unrestricted proposal offered by the OpenSense add-on of the OpenSim musculoskeletal modelling software. Unlike the MVN model, OpenSense enables mastery of both the sensor-to-segment procedure, and the control and constraints of the kinematic chain [12]. The interest of these two models is also their potential integration with musculoskeletal models such as Anybody (AnyBody Technology©) for the MVN model [17] and OpenSim model for its OpenSense add-on.

The lower-body kinematics obtained with IMUs “directly”, i.e., without being submitted to MBO, and kinematics obtained after MBO performed via the MVN and the OpenSense models, were then compared with an optoelectronic-based reference during different tasks. The aim was to estimate the potential of MBO to reduce errors in the lower-body kinematics obtained with IMUs.

2. Material and methods

2.1. Participants

15 asymptomatic subjects – 7 women and 8 men (age: 33.2 ± 9.5 years, mass: 69.6 ± 11.65Kg, size: 171.9 ± 8.24 cm) – took part in this study. All subjects gave their informed consent to participate in the study. The study was reviewed and approved by a Local Ethics Committee.

2.2. Experimental material

The optoelectronic system that served as a reference was composed of 18 cameras (Vicon, Nexus, Oxford, UK) operating at a sampling frequency of 150 Hz. Each subject was equipped with 38 markers but only 28 were used, the lower-limb markers being placed according to the

Table 1
Movement amplitude (in °) authorized at each joint degree of freedom.

Segment	extension or retroversion (-)/flexion or anteversion (+)	abduction or caudal (-) / adduction or cranial (+)	external (-)/internal (+) rotation
Pelvis	-90° /90°	-90° / 90°	-90° / 90°
Hip	-20° / 120°	-45° / 30°	-20° / 20
Knee	-5° / 160°	-15° / 15°	-10° / 10°
Ankle	-40° / 45°	-15° / 15°	-8° / 8°

Conventional Gait Model 2 proposal [18] as illustrated in Fig. 1.

Seven inertial units from the company Xsens were used (Enschede, the Netherlands). The inertial units were positioned on the sacrum, on the lateral side of the thigh on the iliotibial band, on the tibial plateau, and on the anterior part of the midfoot (Fig. 1).

2.3. Protocol

Firstly, postures and movements required for the sensor-to-segment calibration were performed by the subject. This entailed a standing posture with the investigator checking the vertical alignment of the joint centres, followed by a sitting posture: straight leg with both legs held for 5 s. For the Xsens model, the subject performed a static standing posture called "N-pose" then walked a few steps, made a U-turn, and returned to the original position.

Secondly, different functional movements were performed in order to define the joint centres according to the optoelectronic method: a star movement around the hip [19], 5 active knee flexions, and 5 squats.

Finally, the subject performed various movements and physical activities at a pace comfortable for them. Each of the subjects therefore walked and ran on an 8-metre walkway, cycled on an ergocycle for 15 s and finally performed a “sirtaki”. This movement is composed of crossing the feet in front and behind during a lateral movement as shown in Annex 1. This movement was proposed because it is supposed to generate substantial movements in the frontal and transverse planes.

2.4. Kinematics of reference

The marker trajectories were filtered at 20 Hz by a second-order Butterworth low-pass filter. The hip joint centre was obtained by applying the SCORE method [20] to the functional movements that created the hip movements performed in the protocol. The joint axes and centres of the knee and ankle were obtained with the SARA method [21] during leg flexion, squat and lunge movements. The segment coordinate systems were then defined following the recommendations of the International Society of Biomechanics [22] as well as the joint kinematics, which corresponded to the Euler Angles between the joint proximal and distal coordinate systems, following the medio-lateral/antero-posterior/longitudinal axes sequence.

2.5. “Direct” IMU joint kinematics

In order to build each segment coordinate system required to compute the joint kinematics, the following sensor-to-segment calibration method was applied. First, the longitudinal segment axes were considered aligned with gravity, measured by the IMU accelerometers during the standing posture. Then, the medial segment axes were defined as the normalised cross product of the gravity acceleration vector measured during the standing posture and that measured during the sitting posture [23].

The segment coordinate systems were then defined in the underlying IMU coordinate system by taking as first axis the longitudinal axis and, as second axis, the medio-lateral axis. The joint kinematics were then calculated as the Euler angles between the joint proximal and distal coordinate systems following ISB recommendations.

The equations are detailed in Annex 2.

2.6. Xsens MVN kinematics

According to the software procedure, the kinematic chain is first scaled by measuring the subject’s size, foot length, pelvic width (the distance between the two antero-superior iliac spines), and hip, knee, and ankle heights (corresponding respectively to the vertical distance between the ground and the greater trochanter, lateral epicondyle of the femur, and the lateral malleolus).

The exact method used for the sensor-to-segment calibration is not specified. It is only required that the subject adopts a standing posture, walks and performs a U-turn during this step.

In the Xsens MVN kinematic model, 3 degrees of freedom are considered at each lower-limb joint [14]. Neither the constraints nor the optimization process applied to the model are known. The exact procedure used to define the joint kinematics is therefore unknown. The joint kinematics, also expressed as Euler angles, were taken as the outputs of the model.

2.7. OpenSense kinematics and treatment process

The OpenSense multibody kinematics optimization uses a kinematic chain defined by rigid and kinematic constraints that are controlled by IMU quaternions. The model used in this study is a modified version of the Rajagopal model [24]. Degrees of freedom in the frontal and transverse planes of the knee and the ankle joints were unlocked in order to be consistent with the Xsens MVN chain. Thus, each joint was defined as a ball joint. However, a limited amplitude for each degree of freedom was specified according to anatomical data found in the literature [25]. These data are presented in Table 1.

In order to obtain the joint kinematics, a process defined by OpenSense and broken down into three parts must be followed: (1) Data conversion; (2) Calibration of the kinematic chain; (3) Calculation of the kinematics by driving the kinematic chain.

The data conversion step consists of reading the quaternions from the IMUs, specifying the IMU localization on the body segments, and expressing the quaternions in the OpenSim global coordinate system. We chose to transform these quaternions ourselves. For the Xsens IMUs, the Z axis defines the vertical, while in the OpenSense coordinate system it is the Y axis. The IMU quaternions were then reoriented accordingly by performing a 90 ° rotation of the data around the X axis. In the OpenSense process, the relative orientation of the pelvis with respect to the global coordinate system is then sought in order to adapt the orientation of the kinematic chain. For this, the angle between the movement direction and the X axis of the global OpenSim coordinate system must be determined. Following the discovery of some anomalies, we chose to avoid this transformation by adjusting the IMU data ourselves, so that the direction of movement of the kinematic chain was aligned with the X axis of the global OpenSim coordinate system. In order to do this, we assumed that the direction of movement was opposite to the axis perpendicular to the surface of the IMU located at the pelvis, i.e., the pelvis IMU Z axis. The angle between the global X axis and the pelvis IMU Z axis projected onto the horizontal plane was then calculated. From this angle, we constructed a rotation matrix, transformed it into a quaternion and multiplied the quaternion of each IMU by this quaternion. This procedure is detailed in Annex 3.

Next, the OpenSense process performs a sensor-to-segment calibration during the standing posture. By default, the kinematic chain is considered in the anatomical position of reference, therefore the articular angles of the chain are set at 0 °. OpenSense then calculates the transformation between the IMU technical coordinate system and the segment coordinate system. During this step, we modified the joint angles of the kinematic chain during the standing posture by applying the joint angles obtained via the “direct” kinematics procedure (see above). With this method, we could then apply the results of our own sensor-to-

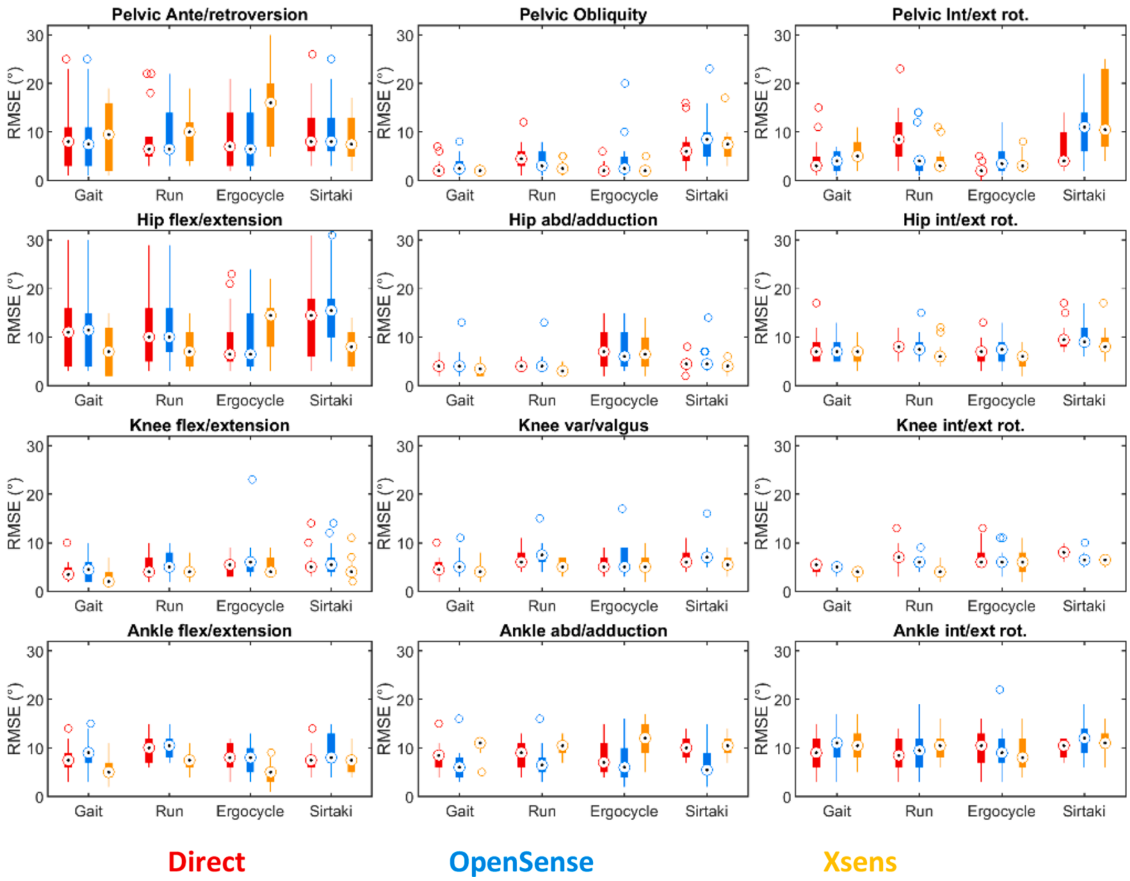

Fig. 2. Root Mean Square Error (RMSE) between the kinematics of reference and the kinematics obtained directly (red), as outputs from the OpenSense (blue) and Xsens (orange) models. On each box, the central mark indicates the median, and the bottom and top edges of the box indicate the 25th and 75th percentiles, respectively. Outliers are represented by circles.

segment calibration procedure.

The last step of the process uses the OpenSim solver to calculate the joint kinematics from the orientations of the inertial units expressed as quaternions and the various constraints included in the model / kinematic chain. It is possible during this step to choose to give more or less importance to the measurement of the orientation of each IMU. We decided to give the same weight to all of the IMUs.

2.8. Data analysis

A comparison was made between the kinematics obtained with the optoelectronic reference and those obtained with the IMUs following the direct procedure (referred to hereafter as "Direct"), the Xsens MVN model (referred to hereafter as "Xsens"), and the OpenSense model (referred to hereafter as "OpenSense"). For this, 2 movement cycles were first extracted on each side. Then, the Root Mean Square Error (RMSE), the Pearson Correlation Coefficient (CC), and the absolute differences in range of motion (RoMdiff) were calculated for each of the 3 kinematics obtained with the IMUs relative to those obtained with the reference, and this for each joint and each of the walking, running, ergocycle, and sirtaki cycle. The results were then averaged for each activity. The CC was not computed for the knee varus/valgus since the evolution of this kinematics can be considered as irrelevant.

2.9. Statistical processing

A Sapiro-Wilk test was used to define the normality of the data. On the RMSE, the CC, and RoMdiff, an ANOVA for repeated measures was performed taking two within-subject factors, the computation method (Direct, OpenSense, and Xsens) and activity (Gait, Run, Ergocyle, and Sirtaki). When the ANOVA showed a p-value of less than 0.05, a Bonferroni Post-hoc test with Bonferroni correction was applied to the data.

3. Results

In Annex 4, the average kinematics across subjects are presented separately for each sports activity. The RMSE are presented in Fig. 2, the CC in Fig. 3, and the RoMdiff in Fig. 4 whereas the results of the ANOVA are presented in Table 2.

For the RMSE, the ANOVA showed an effect of the computation method for pelvis obliquity ($F(2,24) = 5.5$, $p = 0.010$), hip abduction/adduction ($F(2,24) = 3.4$, $p = 0.048$), hip internal/external rotation ($F(2,24) = 4.0$, $p = 0.030$), knee flexion/extension ($F(2,24) = 3.9$, $p = 0.033$) and internal/external rotation ($F(2,24) = 28.4$, $p<0.001$), ankle dorsi/plantarflexion ($F(2,24) = 37.9$, $p<0.001$) and abduction/adduction ($F(2,24) = 11.0$, $p<0.001$). According to the post-hoc tests, the knee internal/external rotation RMSE was significantly greater for the Direct method, followed by the OpenSense method and the Xsens method. For ankle dorsi/plantarflexion, the RMSE was the greatest for the OpenSense method followed by the Direct method and the Xsens method. Finally, for the ankle abduction/adduction, the OpenSense method had a RMSE significantly smaller than the two other methods. For the other kinematics that were significantly affected by the method according to the ANOVA, the multiple pairwise post-hoc tests did not reveal any significance ($p>0.05$). This contradictory result between the ANOVA and the post-hoc tests is probably due to the lack of statistical power.

For the CC, the ANOVA shows an effect of the computation method on pelvic obliquity ($F(3,36) = 10.6$, $p<0.001$), hip internal/external rotation ($F(3,36) = 12.6$, $p<0.001$), knee flexion/extension ($F(3,36) = 5.1$, $p<0.001$), ankle abduction/adduction ($F(3,36) = 13.5$, $p<0.001$)

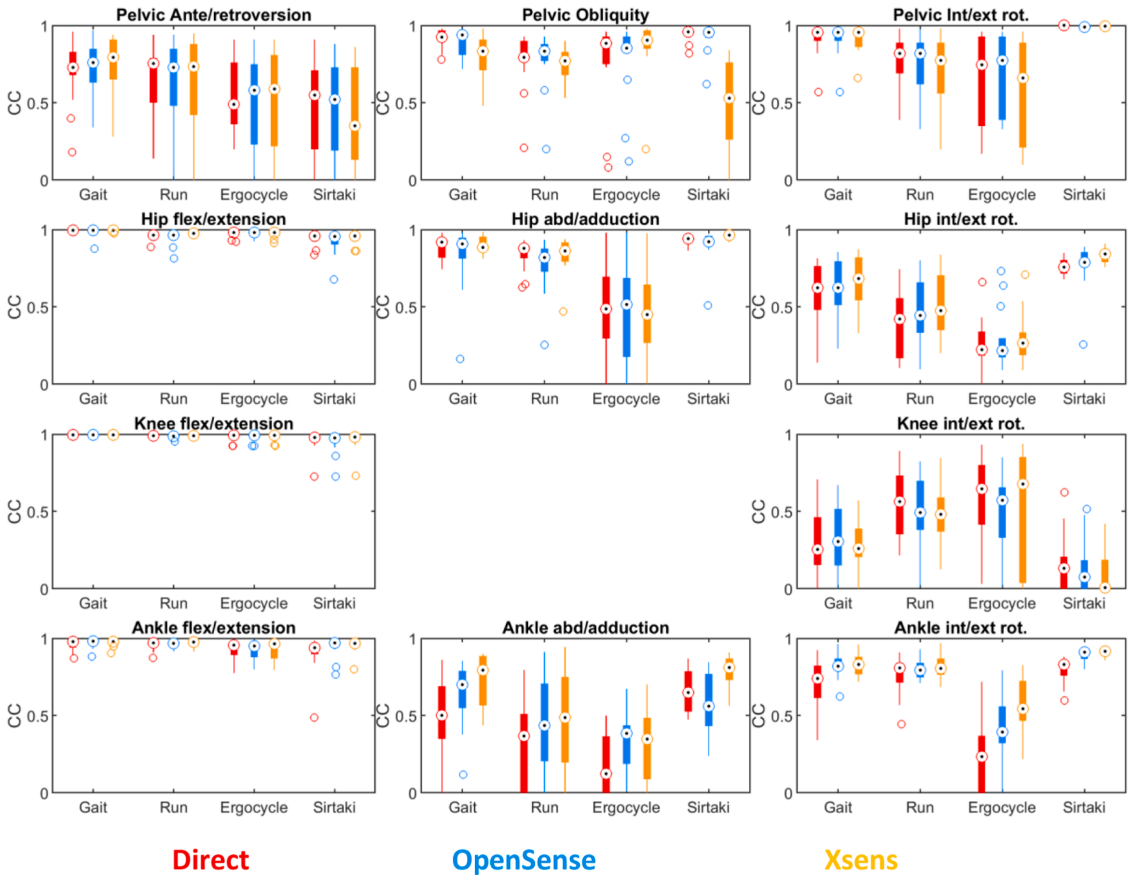

Fig. 3. Correlation Coefficients (CC) between the kinematics of reference and the kinematics obtained directly (red), as outputs from the OpenSense (blue) and Xsens (orange) models. On each box, the central mark indicates the median, and the bottom and top edges of the box indicate the 25th and 75th percentiles, respectively. Outliers are represented by circles.

and internal/external rotation (F(3,36) = 9.3, p<0.001).

According to the post-hoc tests, the Direct and the OpenSense methods had greater CC than the Xsens model for pelvic obliquity. For hip internal/external rotation, ankle abduction/adduction and internal/external rotation, the CC was significantly greater for the Xsens method than for the Direct. For knee flexion/extension, the Xsens method had a greater CC than the OpenSense method.

According to the ANOVA, the method significantly affected the RoMdiff for pelvis ante/retroversion (F(3,36) = 6.8, p = 0.004), knee varus/valgus (F(3,36) = 17.8, p<0.001) and internal/external rotation (F(3,36) = 39.6, p<0.001) as well as for ankle dorsi/plantarflexion (F (3,36) = 8.0, p = 0.002) and abduction/adduction (F(3,36) = 98.8, p<0.001).

According to the post-hoc tests, the RoMdiff was greater for the direct and the OpenSense methods than for the Xsens for pelvis ante/retroversion and knee varus/valgus. For knee internal/external rotation and ankle abduction/adduction the Direct method had the greatest RoMdiff followed by the Xsens. For ankle dorsi/plantarflexion, the Xsens method had a significantly greater value than the Direct method.

As can be noticed in Table 2 the sport activity had many effects on the RMSE, the CC, and the RoMdiff. The sirtaki presenting greater values, for the most part, than other sport activities.

4. Discussion

In this study, the contribution of different MBO methods to obtain lower-limb kinematics with IMUs was evaluated. The hypothesis was made that multi-body optimization could improve the lower-limb kinematics in the frontal and transverse planes comparative to the kinematics directly obtained with IMUs that are particularly prone to the soft-tissue artefact.

The results of the present study are quite similar to the literature for the MVN MBO [4,14] and that of OpenSense [12], considering the differences in methodology or protocol. In the Poitras et al' review [4], which is dedicated to the validity and reliability of wearable sensors for joint angle estimation, different studies that used the MVN system are reported. However, none of the studies present data for each of the lower-body joints during locomotion as does the Schepers et al.' study [14], and no data are presented for cycling or an activity similar to the sirtaki. In the Schepers et al.' study, the kinematics obtained with the MVN model of Xsens were compared to kinematics obtained using an optoelectronic system and subjected to MBO carried out with OpenSim [14]. Their RMSEs evaluated during walking are very similar to those of the present study since their RMSEs were close to 10 ° for hip flexion/extension, 3.2° for knee flexion/extension, and 4.5 ° for ankle dorsi/plantarflexion [14].

The kinematics profile attested by the coefficients of correlation is, in this study, also similar to the literature. In the sagittal plane, for the hip, knee, and ankle joints, they were above 0.90 for all sports activities, but smaller in frontal and transverse planes, as can be seen in Poitras et al' review [4].

Regarding the OpenSense data, we can observe that our RMSEs and correlation coefficients are slightly better than those presented by Al Borno et al. [12]. During walking, their RMSEs are between 3 ° and 6 ° degrees using the Rajagopal kinematic chain [12] and their correlation coefficients - that were presented for only 7 degrees of freedom - did not exceed 0.87. Our results are therefore better, even though we can consider that their reference was more favourable. Firstly, Al Borno et al. used clusters on which markers were attached as well as IMUs. As a result, the movements of the markers tracked by the optoelectronic

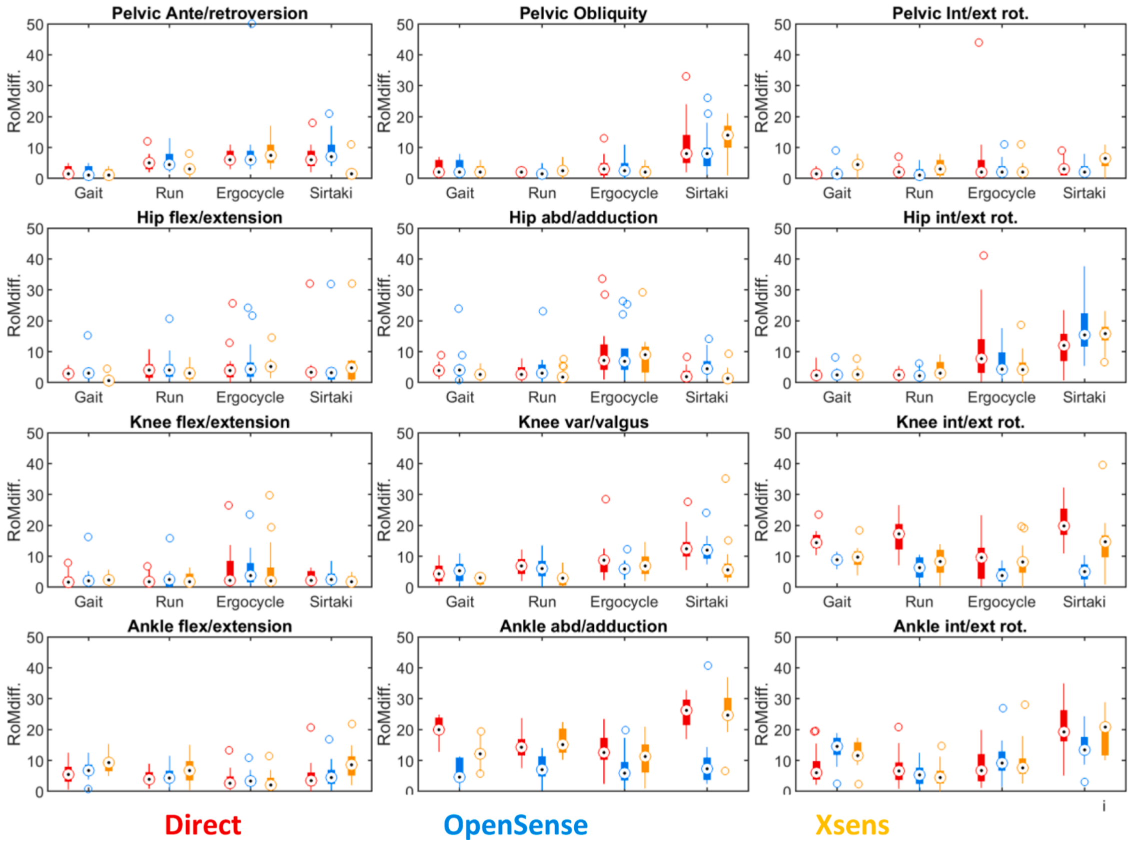

Fig. 4. Range of Motion differences (RoMdiff) between the kinematics of reference and the kinematics obtained directly (red), as outputs from the OpenSense (blue) and Xsens (orange) models. On each box, the central mark indicates the median, and the bottom and top edges of the box indicate the 25th and 75th percentiles, respectively. Outliers are represented by circles.

system underwent the same soft-tissue artefacts as the IMUs. Secondly, the reference kinematics were obtained after MBO performed with the same OpenSim model as that used for the IMU kinematics. Finally, the sensor-to-segment calibration was performed by applying to the kinematic chain the angles obtained by the optoelectronic system during the static position. Another noticeable difference is that Al Borno et al. reduced the relative weighting on the tibial and foot IMUs to minimize the influence of the IMUs that were closer to the ground.

Al Borno et al. [12] observed important errors for the hip rotation (12.7 ° RMSE on average compared to 6.7 ° in the present study), errors assigned to magnetic disturbances by the authors. However, although we observed similar phenomena, our analysis did not confirm that the problem was attributable to magnetic disturbances. In fact, we created quaternions that imitated inertial data using the optoelectronic system, and the problem remained. An anomaly might exist in the way that OpenSense defines the direction of movement which is used by the software to define the initial orientation of the kinematic chain via the pelvis orientation in the global coordinate system. Either that, or we did not manage to apply the procedure correctly. Consequently, we chose to transform the inertial data so that the kinematic chain did not need to be initially rotated in the global frame of reference with the OpenSense procedure.

As found in the literature, the kinematics deteriorate between the sagittal, frontal, and transverse planes, whatever the sports activity. This is partly explained by the fact that the angles are obtained using a Euler sequence around perpendicular axes, whereas the actual functional axes are in fact non-perfectly orthogonal, but this is also true for the reference data. The soft-tissue artefact particularly affects the kinematics in frontal and transverse planes [8] through a “rigid-body translation and rotation component” [26] and, as aforementioned, this artefact is suspected to be greater for the IMU measures than for the optoelectronic. One can also note that the sirtaki shows the worst RMSE, particularly in the transverse plane, which can be explained by the fact that the soft-tissue artefact is activity-dependant [27].

The differences between the kinematics obtained directly and those obtained after MBO are probably not sufficiently relevant judging by the RMSE and the correlation coefficients. For example, for the sirtaki, which presents substantial movements out of the sagittal plane and, as aforementioned, the worst RMSEs, the differences in the RMSE obtained for Direct kinematics and for MBO were smaller than 2° in the frontal and transverse planes. The exception was the pelvis internal/external rotation, for which the RMSE was at least 6° smaller for Direct kinematics than for MBO.

More globally, Xsens optimization seems to present a slight advantage over Direct kinematics or OpenSense optimization, since Xsens presents 34 times out of 48 (12 degrees of freedom * 4 sports activities) a mean RMSE inferior to the Direct and OpenSense kinematics, even though it was not always significant and the differences rarely exceeded 2°. It is also worth mentioning that the Xsens optimization method seems to reduce the outliers as shown in Figs. 2, 3, and 4.

Regarding the advantage of Xsens, the interpretation of the RMSE is, however, problematic since the differences can also originate in the sensor-to-segment calibration. The exact procedure and computation performed during this sensor-to-segment calibration are unknown and could not be replicated with the Direct and OpenSense procedures. It is then intriguing that the RMSEs were, for instance, close to the Direct kinematics for running with pelvis ante/retroversion and knee flexion/extension, showing less than 1° difference in RMSE but as much as 5° for hip flexion/extension. One could expect to also perceive some differences in a hip-adjacent joint. The sensor-to-segment calibration procedure applied to the pelvis was also not optimal for the Direct and the OpenSense data. According to a study performed in our laboratory, the

Table 2
Results of the ANOVA for repeated measures statistical test and Bonferroni Post-hoc test applied to the Root Mean Square Error (RMSE), the correlation coefficients (CC), and Range of Motion differences (RoMdiff) taking two within-subject factors, the computation method (Direct “D”, OpenSense, “O”, and Xsens “X”), and activity (Gait “G”, Run “R”, Ergocyle “E”, and Sirtaki “S”). When significant, the p-values have been inserted in bold. Regarding the post-hoc results, M1>M2>M3 means for example that method M1 has results statistically superior to the results of the M2 and M3 methods and that the method M2 has results statistically superior to the results of the method M3. Note that for some data significantly affected by the method or activity, the multiple pairwise post-hoc tests did not reveal any significance.

				Pelvis			Hip			Knee			Ankle	
			ant/retro	obl	int/ext rot	flex/ext	abd/add	int/ext rot	flex/ext	var/val	int/ext rot	flex/ext	abd/add	int/ext rot
RMSE	Method	**F (2,24)**	0.2	5.5	1.0	1.4	3.4	4.0	3.9	3.4	28.4	37.9	11.0	0.7
		p-value	0.828	**0.010**	0.370	0.258	**0.048**	**0.030**	**0.033**	0.050	**0.000**	**0.000**	**0.000**	0.522
		post-hoc									*D>O>X*	*O>D>X*	D,*X>O*	
	Activity	**F (3,36)**	0.9	19.4	1.8	3.7	9.6	7.1	4.2	8.1	11.9	20.6	0.8	4.3
		p-value	0.461	**0.000**	0.173	**0.020**	**0.000**	**0.001**	**0.012**	**0.000**	**0.000**	**0.000**	0.492	**0.010**
		post-hoc		*G,R, E<S*		*G<S*	*G,R <E*	*G,R <S*	*G<E*	*G<R, E*	*G<S,R,E; R<S*	*G,S,E<R; E<S*		*R<S*
CC	Method	**F (2,24)**	0.8	10.6	0.8	2.6	1.4	12.6	5.1	3.6	2.3	2.3	13.5	9.3
		p-value	0.476	**0.000**	0.450	0.097	0.264	**0.000**	**0.014**	0.040	0.125	0.121	**0.000**	**0.001**
		post-hoc		*D,O>X*				*X>D*	*X>O*	*D>X*			*X>D*	*X>D*
	Activity	**F (3,36)**	3.2	1.6	10.1	10.3	26.2	23.0	3.3	9.1	10.4	2.0	17.2	65.0
		p-value	**0.034**	0.199	**0.000**	**0.000**	**0.000**	**0.000**	**0.031**	**0.000**	**0.000**	0.136	**0.000**	**0.000**
		post-hoc	*S<G*	*S<G*	*R,E<S*	*R,S<G*	*E<G,R,S; R<S*	*R,E<G, S*	*R<G*	*R<G,S*	*G,S<R; S<E*		*E<G,S; R<S*	*E<G,R<S*
RoMdiff	Method	**F (2,24)**	6.8	1.1	1.5	2.4	2.9	0.0	0.1	17.8	39.6	8.0	98.8	0.3
		p-value	**0.004**	0.363	0.237	0.112	0.075	0.975	0.893	**0.000**	**0.000**	**0.002**	**0.000**	0.714
		post-hoc									*D>O>X*	*O>D>X*	*X>O*	
	Activity	**F (3,36)**	9.9	26.8	1.7	1.3	7.9	9.5	0.8	12.3	4.5	5.6	16.0	14.8
		p-value	**0.000**	**0.000**	0.177	0.287	**0.000**	**0.000**	0.504	**0.000**	**0.008**	**0.003**	**0.000**	**0.000**
		post-hoc	*G<R,S, E*	*R,G, E<S*			*R<E*	*R,G<S*		*R,G<S*	*E<G*	*R,E<G*	*R,G, E<S*	*R<G<S; E<S*

best method for the pelvis uses a device equipped with an IMU that enables pinpointing of the iliac spines. But in order to be as close as possible to the MVN model, it was decided not to apply this method. It is expected then, that the pelvis and the hip Direct and OpenSense kinematics would be better when applying this specific sensor-to-segment calibration to the pelvis.

The limited effect of MBO can also be explained by several factors. Firstly, it should be noted that for the MVN and the OpenSense model 3 degrees of freedom were considered at each joint. However, to reduce the soft-tissue artefacts, there is a need to constrain the degrees of freedom [29]. The lack of influence of the MBO could therefore be partly explained by the absence of kinematic constraints. We tested another version of the Rajagopal model by defining 2 degrees of freedom at the knees and one at the ankles. Only hip abduction/adduction was improved, as attested by a smaller RMSE and a greater correlation coefficient found for this model than for the 3 degrees of freedom model. The definition of the joints seems therefore to have a limited effect. A more “physiological” definition of the joints could be significant [28-31]. However, more complex joints might be problematic to drive with IMUs.

The low contribution of MBO could also be explained by the fact that the segment orientation serving as input comes from a single IMU fixed on the segment and not, as for optoelectronic systems, from several markers distributed over the segment. The so-called rigid constraint, which considers that all the points of measurement of a segment are rigidly linked, does not therefore exist here. The “rigid-body translation and rotation component” of the soft-tissue artefact can probably not be prevented with only one point of measurement by segment, especially with a 3 degrees of freedom joint model. The use of more than two IMUs per segment might be a possibility to provide measure redundancy in order to exploit a rigid constraint, but it would be to the detriment of wearability.

In fact, performing MBO via IMU orientation might not be the most adequate solution. It is also possible to reconstruct the movement by defining a Kalman filter that integrates state variables based on biomechanical constraints or a kinematic chain [9,30]. This approach seems particularly adequate when using IMUs since the IMU orientations are obtained by sensor-fusions algorithms such as Kalman filters.

For the OpenSense model, it was decided to impose range-of-motion limits based on the work of Kapandji [25]. For the Xsens model, it is possible to reprocess the data by applying different scenarios (for instance, the low-level or the no-level scenario), which seems to also influence the range of motion, since saturation in knee flexion was apparent. With the OpenSense model, saturation phenomena were also observed, particularly in knee varus/valgus and rotation. By looking at the kinematics of reference, the saturation makes sense in preventing the achievement of inappropriate range of motion and this can explain the (relatively small) improvement of the kinematics obtained after multi-body optimization. However, it would be interesting to enter limits tailored to the subject studied.

Of course, an important issue with regard to the present discussion of the results, is that these results suffer from a significant drawback: they are obtained by taking optoelectronic system measures as reference. The optoelectronic system methodology based on external markers does not constitute a "gold standard" in medical imagery, but rather a “silver standard”. As mentioned in the introduction, it is well known that the resulting kinematics are subject to many errors, such as the soft-tissue artefact, marker misplacement, or the localization of the joint centres [5–7].

5. Conclusion

This study does not conclude that MBO makes a very significant contribution to improving lower-body kinematics obtained with IMUs. This lack of results can partly be explained by the weakness of the kinematic constraints applied to the kinematic chain (3 degrees of freedom existed at the joints) and of segment stiffening. The results also highlight that sensor-to-segment calibration remains essential for obtaining these kinematics. Personalization of the kinematic chain in terms of range of motion, type of joint, and calibration, could improve the kinematics as well as the use of more than one sensor by segment in order to provide information redundancy. Other approaches based on the Kalman Filter might, in fact, be more adequate to integrate biomechanical constraints when using IMUs to obtain lower-body kinematics.

Funding

This study was supported in part by the New Aquitaine region and the European Union through the Habisan program (CPER-FEDER).

Ethical approval

Subjects gave written informed consent prior to their participation. The study was reviewed and approved by a Local Ethics Committee. Work on human beings that is submitted to *Medical Engineering & Physics* should comply with the principles laid down in the Declaration of Helsinki; Recommendations guiding physicians in biomedical research involving human subjects. Adopted by the 18th World Medical Assembly, Helsinki, Finland, June 1964, amended by the 29th World Medical Assembly, Tokyo, Japan, October 1975, the 35th World Medical Assembly, Venice, Italy, October 1983, and the 41st World Medical Assembly, Hong Kong, September 1989. You should include information as to whether the work has been approved by the appropriate ethical committees related to the institution(s) in which it was performed and that subjects gave informed consent to the work.

Declaration of Competing Interest

The authors declare no conflict of interest. The funders had no role in the design of the study; in the collection, analyses, or interpretation of data; in the writing of the manuscript, or in the decision to publish the results.

Acknowledgement

The authors would like to thank the subjects who took part in the study as well as Mrs Hogan for the English proofreading.

Supplementary materials

Supplementary material associated with this article can be found, in the online version, at doi:10.1016/j.medengphy.2022.103927.

ANNEX 1: Illustration of the sirtaki

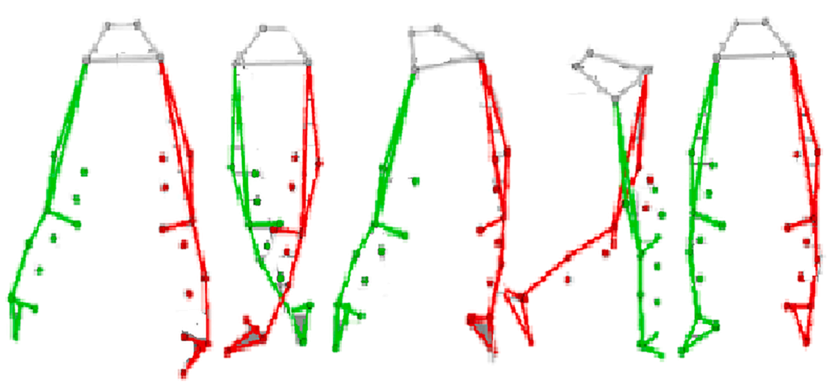

ANNEX 2: Sensor to segment calibration and direct kinematics

For the standing posture, for which the longitudinal axes of the segments are considered to be aligned with the vertical and positive upwards, the vertical is defined in the technical coordinate system of the IMU, based on the acceleration vector assumed to correspond to gravity $\vec{g}$ given by the measurement of the following accelerometer as (1):

$$\vec{e}^{\,IMU}_{Lstanding} = mean\left(- \vec{g}^{\,IMU} \right) \tag{1}$$

$\vec{e}^{\,IMU}_{L\ standing}$ is then normalized. This mean normalized acceleration vector is also calculated for the seated position to obtain $\vec{e}^{\,IMU}_{V\ Sitting}$. The medio-lateral axes of the pelvis, femurs, tibias and feet $\vec{e}^{\,IMU}_{ML}$, are then defined as the cross product of the vertical vectors obtained during the standing and sitting postures as follows (2).

$$\vec{e}^{\,IMU}_{ML} = \vec{e}^{\,IMU}_{LStanding} \times \vec{e}^{\,IMU}_{VSitting} \tag{2}$$

For the inertial units, as for the reference, the segment coordinate systems expressed in the technical coordinate system of the IMUs R_{seg}^{IMU} are defined by a main vector and a secondary vector. For the pelvis, the main vector is defined as the medio-lateral vector $\overrightarrow{e}_{ML}^{IMU_{pelvis}}$, the secondary vector is the longitudinal vector $\overrightarrow{e}_{L}^{IMU_{pelvis}}$. For the other segments, the main vector is the longitudinal vector $\overrightarrow{e}_{L}^{IMU}$ and the secondary vector is the medio-lateral vector $\overrightarrow{e}_{ML}^{IMU}$. The first axis of the coordinate system is therefore defined by the principal vector, the second axis by the vector product of the principal and secondary vectors, while the third is defined as the vector product of the first and second axes as follows (3), (4), and (5).

$$R_{seg}^{IMU}\begin{cases}\overrightarrow{e_L^{IMU}} = \overrightarrow{e_L^{IMU}} & (3)\\ \overrightarrow{e_{AP}^{IMU}} = \overrightarrow{e_{ML}^{IMU}} \wedge \overrightarrow{e_L^{IMU}} & (4)\\ \overrightarrow{e_{ML}^{IMU}} = \overrightarrow{e_L^{IMU}} \wedge \overrightarrow{e_{AP}^{IMU}} & (5)\end{cases} \tag{3}$$

The axes thus obtained make it possible to construct the rotation matrix giving the orientation of the segment coordinate system in the technical coordinate system of the IMUs. This matrix is then expressed as a quaternion q_{seg}^{IMU} using the SpinCalc function on MATLAB (Fuller, 2021). During the movements studied, in order to obtain the joint kinematics, whether from the IMUs or the optoelectronic system, the relative orientation between the proximal and the distal segment coordinate systems is calculated in the form of quaternions. For the inertial data, we define first, at each instant, the segment coordinate systems expressed in the global coordinate system of the IMUs as (6):

$$q_{seg}^{O_{IMU}}(t) = q_{IMU}^{O_{IMU}}(t) \otimes q_{seg}^{IMU}(t) \tag{6}$$

Then we define the relative quaternion between the two adjacent segments surrounding the joint as (7):

$$q_{prox}^{dist}(t) = q_{dist}^{O_{IMU}}(t)^{*} \otimes q_{prox}^{O_{IMU}}(t) \tag{7}$$

The quaternion formalism was chosen because the computation time is much faster. This quaternion was then decomposed into a Euler sequence as recommended by the ISB (Wu et al., 2002), still using the SpinCalc function on MATLAB.

ANNEX 3: Transformation of the inertial data for the OpenSense model

For the OpenSim model, the vertical axis positive upwards is the $\overrightarrow{Y}$ axis whereas it is the $\overrightarrow{Z}$ axis for the IMU global coordinate system. The quaternions measured by the IMUs were first reoriented in the OpenSim coordinate system frame by performing the operation as follows (8):

$$q_{IMU}^{O_{OpenSense}} = q_{O_{IMU}}^{O_{OpenSense}} \times q_{IMU}^{O_{IMU}} \tag{8}$$

with $q_{O_{IMU}}^{O_{OpenSense}} = \begin{bmatrix}0.7071\\0\\0\\0.7071\end{bmatrix}$ in order to define a 90° rotation of IMU data around the $\overrightarrow{X}$ axis.

The OpenSense workflow reorients the kinematic chain by aligning the antero-posterior axis of the pelvis coordinate system with the movement direction. However, this step presents some unexplained anomalies. Therefore, we chose to circumvent this step by rotating the IMU data such that the antero-posterior axis of the pelvis was aligned to the $\overrightarrow{X}$ axis of the OpenSim global coordinate system.

We first determined the angle between the antero-posterior axis of the pelvis and the $\overrightarrow{X}$ axis of the OpenSim global coordinate system by assuming that the antero-posterior axis of the pelvis was opposite to the axis perpendicular to the surface of the IMU placed on the pelvis (with the Xsens IMUs, it corresponds to the axis $\overrightarrow{Z}_{IMU_{Pelvis}}^{O_{OpenSense}}$) at the beginning of the movement. We calculated the angle θ between $\overrightarrow{X}_{O_{OpenSense}}$ and the projected of $-\overrightarrow{Z}_{IMU_{Pelvis}}^{O_{OpenSense}}$ in the horizontal plane of the OpenSim global coordinate system as follows (9):

$$\theta = a\tan 2\left(\frac{-\overrightarrow{Z}_{p\,IMU_{Pelvis}}^{O_{OpenSense}} \cdot \overrightarrow{X}_{O_{OpenSense}}}{\|\overrightarrow{Z}_{p\,IMU_{Pelvis}}^{O_{OpenSense}}\| \times \|\overrightarrow{X}_{O_{OpenSense}}\|}, \frac{\|\overrightarrow{Z}_{p\,IMU_{Pelvis}}^{O_{OpenSense}} \times \overrightarrow{X}_{O_{OpenSense}}\|}{\|\overrightarrow{Z}_{p\,IMU_{Pelvis}}^{O_{OpenSense}}\| \times \|\overrightarrow{X}_{O_{OpenSense}}\|}\right) \tag{9}$$

From this angle, we obtained the rotation matrix used to rotate all the IMU data as (10):

$$M_{dir\ mvt} = \begin{Bmatrix} cos\theta & 0 & sin\theta \\ 0 & 1 & 0 \\ -sin\theta & 0 & cos\theta \end{Bmatrix} \tag{10}$$

This rotation matrix was then transformed into a quaternion $q_{dir\,mvt}$ using the SpinCalc function (Fuller, 2021) and applied to each of the quaternions of the IMUs as in (11):

$$q_{IMU_{rotated}}^{O_{OpenSense}} = q_{dir\ mvt} \times q_{IMU}^{O_{IMU}} \tag{11}$$

ANNEX 4: Mean joint kinematics for the different sports activities

Fig. A4-1, Fig. A4-2, Fig. A4-3, Fig. A4-4

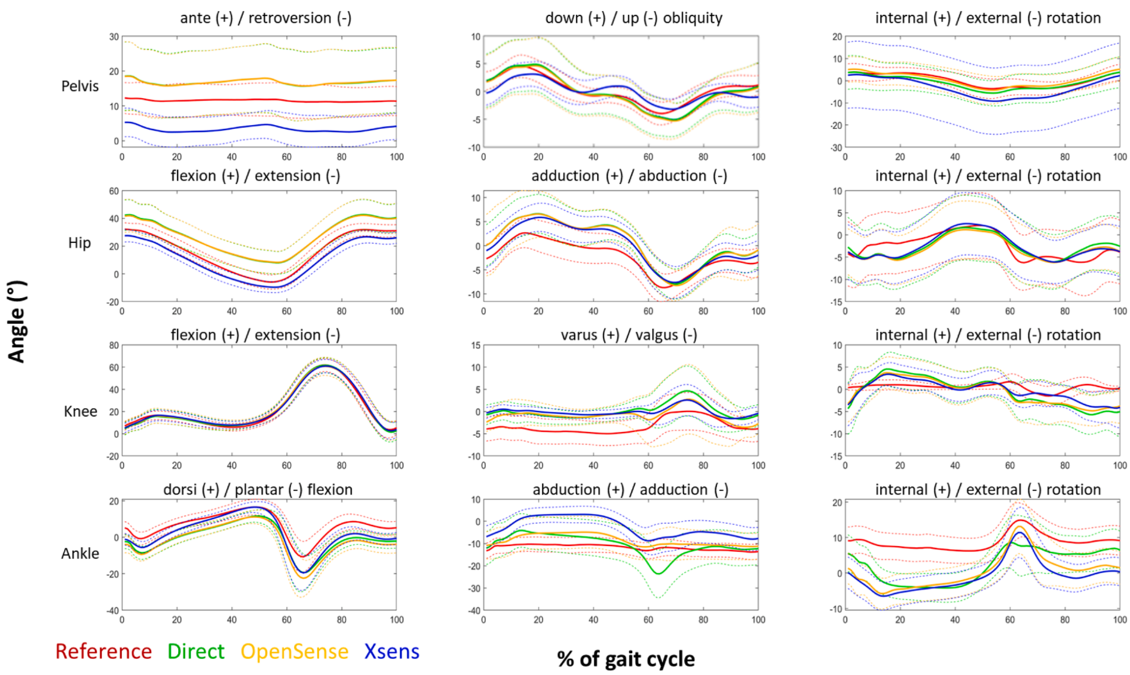

Fig. A4–1. Mean kinematics obtained during a gait cycle. The reference kinematic is in red, the direct kinematic in green, the Xsens kinematic in blue, and the OpenSense kinematic in yellow. The dotted lines represent the standard deviation across the subjects.

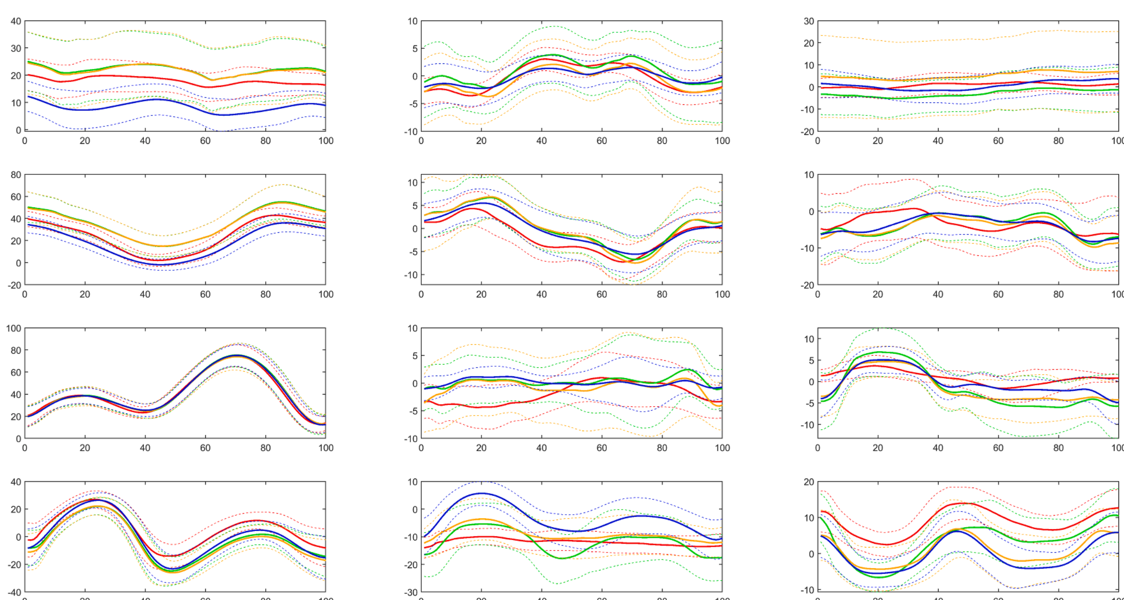

Fig. A4–2. Mean kiematics obtained during a running cycle. The reference kinematic is in red, the direct kinematic in green, the Xsens kinematic in blue, and the OpenSense kinematic in yellow. The dotted lines represent the standard deviation across the subjects.

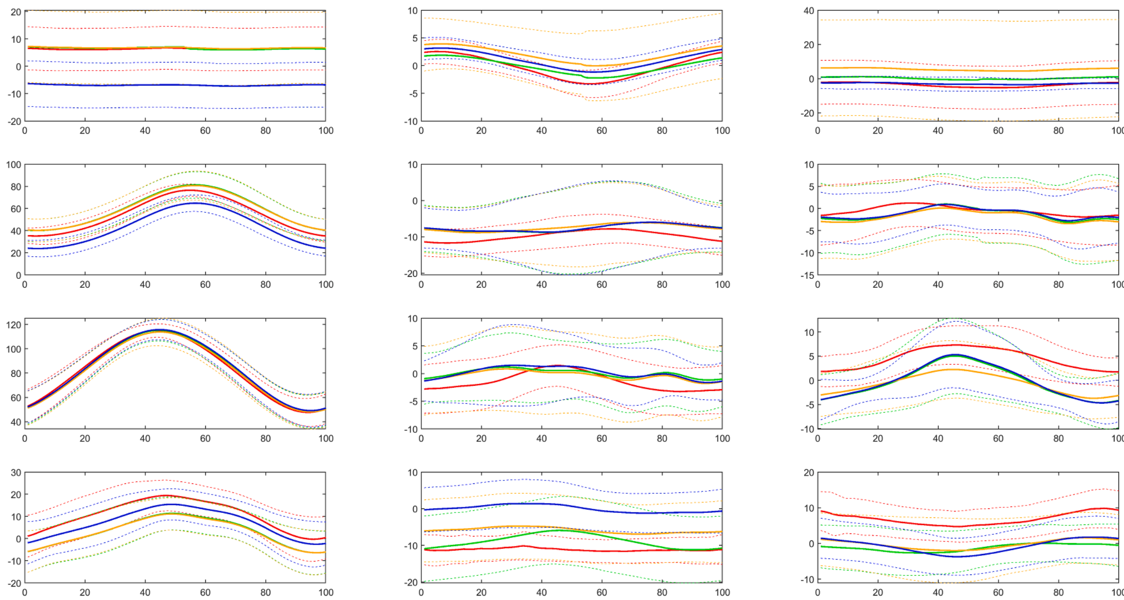

Fig. A4–3. Mean kinematics obtained during an ergocycle cycle. The reference kinematic is in red, the direct kinematic in green, the Xsens kinematic in blue, and the OpenSense kinematic in yellow. The dotted lines represent the standard deviation across the subjects.

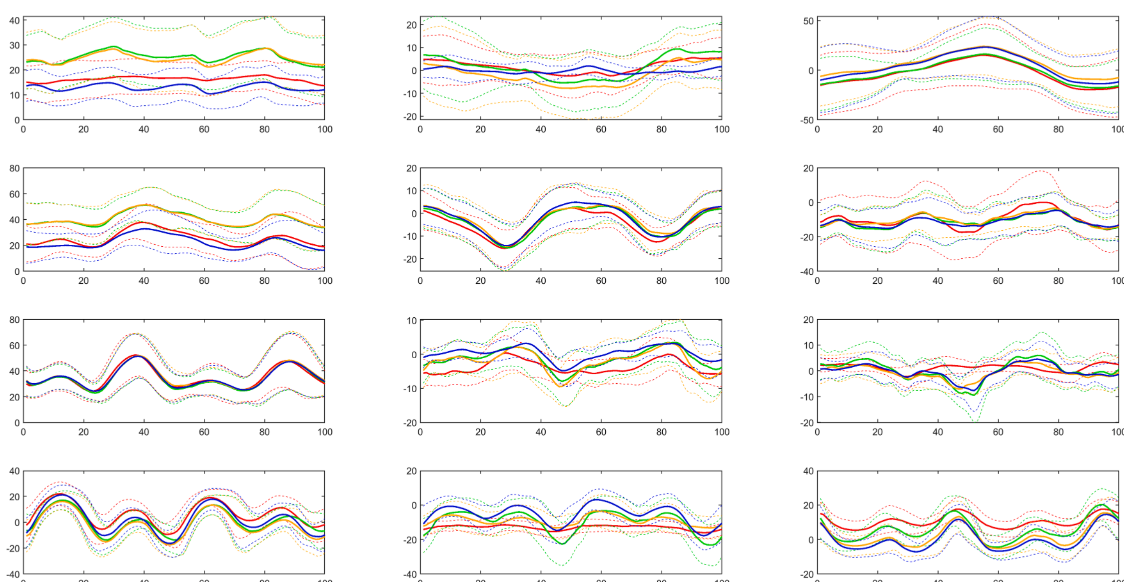

Fig. A4–4. Mean kinematics obtained during a sirtaki cycle. The reference kinematic is in red, the direct kinematic in green, the Xsens kinematic in blue, and the OpenSense kinematic in yellow. The dotted lines represent the standard-deviation across the subjects.

References

[1] Ghattas J, Jarvis DN. Validity of inertial measurement units for tracking human motion: a systematic review. Sports Biomech 2021;0:1–14. https://doi.org/10.1080/14763141.2021.1990383.

[2] Picerno P, Iosa M, D'Souza C, Benedetti MG, Paolucci S, Morone G. Wearable inertial sensors for human movement analysis: a five-year update. Expert Rev Med Devices 2021;18:79–94. https://doi.org/10.1080/17434440.2021.1988849.

[3] Pacher L, Chatellier C, Vauzelle R, Fradet L. Sensor-to-segment calibration methodologies for lower-body kinematic analysis with inertial sensors: a systematic review. Sensors 2020;20:3322. https://doi.org/10.3390/s20113322.

[4] Poitras I, Dupuis F, Bielmann M, Campeau-Lecours A, Mercier C, Bouyer LJ, et al. Validity and reliability of wearable sensors for joint angle estimation: a systematic review. Sensors 2019;19:E1555. https://doi.org/10.3390/s19071555.

[5] Leardini A, Chiari L, Della Croce U, Cappozzo A. Human movement analysis using stereophotogrammetry. Part 3. Soft tissue artifact assessment and compensation. Gait Posture 2005;21:212–25. https://doi.org/10.1016/j.gaitpost.2004.05.002.

[6] Della Croce U, Leardini A, Chiari L, Cappozzo A. Human movement analysis using stereophotogrammetry. Part 4: assessment of anatomical landmark misplacement and its effects on joint kinematics. Gait Posture 2005;21:226–37. https://doi.org/10.1016/j.gaitpost.2004.05.003.

[7] Kainz H, Graham D, Edwards J, Walsh HPJ, Maine S, Boyd RN, et al. Reliability of four models for clinical gait analysis. Gait Posture 2017;54:325–31. https://doi.org/10.1016/j.gaitpost.2017.04.001.

[8] Stagni R, Fantozzi S, Cappello A, Leardini A. Quantification of soft tissue artefact in motion analysis by combining 3D fluoroscopy and stereophotogrammetry: a study on two subjects. Clin Biomech Bristol Avon 2005;20:320–9. https://doi.org/10.1016/j.clinbiomech.2004.11.012.

[9] Begon M, Andersen MS, Dumas R. Multibody kinematics optimization for the estimation of upper and lower limb human joint kinematics: a systematized methodological review. J Biomech Eng 2018;140. https://doi.org/10.1115/1.4038741.

[10] Lu TW, O'Connor JJ. Bone position estimation from skin marker co-ordinates using global optimization with joint constraints. J Biomech 1999;32:129–34.

[11] Delp SL, Anderson FC, Arnold AS, Loan P, Habib A, John CT, et al. OpenSim: open-source software to create and analyze dynamic simulations of movement. IEEE Trans Biomed Eng 2007;54:1940–50. https://doi.org/10.1109/TBME.2007.901024.
[12] Al Borno M, O'Day J, Ibarra V, Dunne J, Seth A, Habib A, et al. OpenSense: an open-source toolbox for inertial-measurement-unit-based measurement of lower extremity kinematics over long durations. J NeuroEng Rehabil 2022;19:22. https://doi.org/10.1186/s12984-022-01001-x.
[13] Cooper G, Sheret I, McMillan L, Siliverdis K, Sha N, Hodgins D, et al. Inertial sensor-based knee flexion/extension angle estimation. J Biomech 2009;42:2678–85.
[14] Schepers M., Giuberti M., Bellusci G. Xsens MVN: consistent tracking of human motion using inertial sensing 2018. https://doi.org/10.13140/RG.2.2.22099.07205.
[15] Al-Amri M, Nicholas K, Button K, Sparkes V, Sheeran L, Davies JL. Inertial measurement units for clinical movement analysis: reliability and concurrent validity. Sensors 2018;18. https://doi.org/10.3390/s18030719.
[16] Zhang J-T, Novak AC, Brouwer B, Li Q. Concurrent validation of Xsens MVN measurement of lower limb joint angular kinematics. Physiol Meas 2013;34:N63–9. https://doi.org/10.1088/0967-3334/34/8/N63.
[17] Konrath JM, Karatsidis A, Schepers HM, Bellusci G, de Zee M, Andersen MS. Estimation of the knee adduction moment and joint contact force during daily living activities using inertial motion capture. Sensors 2019;19:1681. https://doi.org/10.3390/s19071681.
[18] Leboeuf F, Baker R, Barré A, Reay J, Jones R, Sangeux M. The conventional gait model, an open-source implementation that reproduces the past but prepares for the future. Gait Posture 2019. https://doi.org/10.1016/j.gaitpost.2019.04.015.
[19] Camomilla V, Cereatti A, Vannozzi G, Cappozzo A. An optimized protocol for hip joint centre determination using the functional method. J Biomech 2006;39:1096–106.
[20] Halvorsen K. Bias compensated least squares estimate of the center of rotation. J Biomech 2003;36:999–1008.
[21] Ehrig RM, Taylor WR, Duda GN, Heller MO. A survey of formal methods for determining functional joint axes. J Biomech 2007;40:2150–7. https://doi.org/10.1016/j.jbiomech.2006.10.026.
[22] Wu G, Siegler S, Allard P, Kirtley C, Leardini A, Rosenbaum D, et al. ISB recommendation on definitions of joint coordinate system of various joints for the reporting of human joint motion–part I: ankle, hip, and spine. International Society of Biomechanics. J Biomech 2002;35:543–8.
[23] Tadano S, Takeda R, Miyagawa H. Three dimensional gait analysis using wearable acceleration and gyro sensors based on quaternion calculations. Sensors 2013;13:9321–43. https://doi.org/10.3390/s130709321.
[24] Rajagopal A, Dembia CL, DeMers MS, Delp DD, Hicks JL, Delp SL. Full-body musculoskeletal model for muscle-driven simulation of human gait. IEEE Trans Biomed Eng 2016;63:2068–79. https://doi.org/10.1109/TBME.2016.2586891.
[25] Kapandji AI. Anatomie fonctionnelle - Tome 2 - Membre inférieur. Maloine; 2018.
[26] Andersen MS, Damsgaard M, Rasmussen J, Ramsey DK, Benoit DL. A linear soft tissue artefact model for human movement analysis: proof of concept using in vivo data. Gait Posture 2012;35:606–11. https://doi.org/10.1016/j.gaitpost.2011.11.032.
[27] Akbarshahi M, Schache AG, Fernandez JW, Baker R, Banks S, Pandy MG. Non-invasive assessment of soft-tissue artifact and its effect on knee joint kinematics during functional activity. J Biomech 2010;43:1292–301. https://doi.org/10.1016/j.jbiomech.2010.01.002.
[28] Pacher L, Chatellier C, Laguillaumie P, Vauzelle R, Fradet L. Lower Limb Sensor-to-Segment Calibration for Joint Kinematics Analysis With Inertial Measurement Units: Is There an Ideal Method? IEEE Sensors Journal 2022;22(22):22148–60. https://doi.org/10.1109/JSEN.2022.3209883.
[29] Gasparutto X, Sancisi N, Jacquelin E, Parenti-Castelli V, Dumas R. Validation of a multi-body optimization with knee kinematic models including ligament constraints. J Biomech 2015;48:1141–6. https://doi.org/10.1016/j.jbiomech.2015.01.010.
[30] Duprey S, Cheze L, Dumas R. Influence of joint constraints on lower limb kinematics estimation from skin markers using global optimization. J Biomech 2010;43:2858–62. https://doi.org/10.1016/j.jbiomech.2010.06.010.
[31] Miezal M, Taetz B, Bleser G. On inertial body tracking in the presence of model calibration errors. Sensors 2016;16. https://doi.org/10.3390/s16071132.